Journal of Advance in Natural Science and Engineering
March, 2025; Volume 1, Number 1, Pages 17 - 32
https://doi.org/10.5281/zenodo.16879008

Design and Simulation-Based Performance Analysis of A PIC16F73 Microcontroller-Based Solar Charge Controller For Power Solutions In Federal University Otuoke

Ifeagwu E. N.
Department of Electrical & Electronic Engineering, Federal University Otuoke, Bayelsa State
*Corresponding author's email address: ifeagwuen@fuotuoke.edu.ng

Abstract: This paper focuses on the design and simulation-based performance analysis of a PIC16F73 microcontroller-based solar charge controller for power solutions in Federal University Otuoke. A 12V microcontroller-based charge controller was designed and simulated to achieve this objective. Given the abundant sunlight in the region, the study centred on a solar power system, which generates electrical energy from sunlight using photovoltaic (PV) panels. Since solar energy is unavailable at night, a battery storage system is required to store energy harvested during the day. The charge controller serves as a critical component of the solar power system, regulating and monitoring the battery's charging and discharging processes. The proposed system comprises five functional units: a current booster, a switching unit, a control unit, a voltage sensing unit, and a voltage regulation unit. The controller was developed using a 28-pin PIC16F73 microcontroller, selected for its ease of use, configuration, and programmability. It can handle up to 23A. The entire design process was implemented and simulated using MATLAB/Simulink.

Keywords: MATLAB/Simulink, microcontroller, battery, performance, solar power system

Cite: Ifeagwu E. N.(2025). Design and Simulation-Based Performance Analysis Of A PIC16F73 Microcontroller-Based Solar Charge Controller for Power Solutions in Federal University Otuokes Journal of Advance in Natural Science and Engineering Volume 1(1): Pages 17 – 32; tps://doi.org/10.5281/zenodo.16879008

Introduction

Nigeria continues to grapple with the challenge of unreliable electricity and frequent power outages, making alternative energy solutions essential. The Federal University Otuoke (FUO) is equally affected by this power crisis. Due to the lack of grid power within the university community, FUO depends entirely on generators to meet its electricity needs. To address this challenge, the Department of Electrical and Electronic Engineering has embraced renewable energy solutions to achieve a sustainable and reliable power supply.

Among the available renewable energy sources, solar energy has proven to be the most feasible option for alternative power supply solutions (IEA, 2021). The sun emits approximately 180 billion megawatts (MW) of energy to the Earth, and just one hour of this energy is enough to meet the world's electricity demand for an entire year (Khan *et al*, 2016). Solar energy is clean, non-polluting, inexhaustible, and abundantly available.

A standard solar power system comprises photovoltaic (PV) panels, a charge controller, a battery, and an inverter (Osaretin & Edeko, 2015). PV panels convert sunlight into electrical voltage and current. However, under intense solar radiation, these panels may generate voltages higher than the battery's rated capacity, risking overcharging and damage. To efficiently capture and regulate solar energy, an advanced energy management system is required.

To address this challenge, a performance analysis of a microcontroller-based charge controlling unit becomes necessary. This device regulates voltage and current to prevent battery overcharging and optimize energy extraction from solar panels. Overcharging occurs when a battery receives more current than it can safely store.

Every battery has a maximum current threshold; exceeding it causes grid corrosion and electrolyte loss. When excess current flows, the electrolyte decomposes into hydrogen and oxygen gases, a process known as gassing (Kibirige *et al*., 2024). This gas loss is typically irreversible unless recombined into water, and continuous electrolyte evaporation results in permanent capacity loss.

The microcontroller-based device is designed to maximize power extraction from the PV array, fully charge the batteries, and prevent unwanted discharge at the set point—all without self-power consumption. It also blocks reverse current flow. The charge controller is fully configurable to meet industry standards and ensure maximum PV system efficiency. When connected to solar panels and batteries, it automatically optimizes charging by utilizing all available solar energy.

Journal of Advance in Natural Science and Engineering
March, 2025; Volume 1, Number 1, Pages 17 - 32
https://doi.org/10.5281/zenodo.16879008

Additionally, the solar microcontroller-based charge controller features an advanced three-stage charging mechanism, which can be tailored to specific battery requirements (Osaretin & Edeko, 2015). It integrates multiple protective measures against voltage surges, overheating, overcurrent, reverse battery polarity, and reverse PV connections. Its automatic current-limiting feature allows full-capacity operation without risk of overload from excessive current, voltage, or amp-hour-based load conditions (Santos *et al.*, 2019).

This innovative solution offers a reliable and efficient approach to addressing FUO's energy challenges while promoting sustainable power usage.

Some previous works were reviewed and summarized as follows**:**

The research titled "Design and Implementation of a Microcontroller-Based Solar Battery Charger by Nwankwo *et al.* (2021)" illustrated that both systems utilize PWM for charge regulation; however, Nwankwo *et al.* (2021) incorporate temperature compensation, enhancing charging efficiency and battery lifespan—a feature not addressed in the PIC16F73-based system. Additionally, while the Arduino Uno (ATmega328P) used by Nwankwo supports rapid prototyping due to its accessibility and ease of use, the PIC microcontroller is typically favored for industrial-grade applications. Notably, Nwankwo's study is based on practical hardware implementation and testing, in contrast to the simulation-based approach of the FUO paper.

The paper by Adamu *et al.* (2022) on "Development of a Smart Solar Charge Controller Using MPPT and IoT" developed a smart solar charge controller using the ESP32 microcontroller, which integrates Wi-Fi for IoT connectivity and employs MPPT (Maximum Power Point Tracking) for higher efficiency under varying sunlight conditions—significantly outperforming the PWM-based method used in the FUO study. Unlike the FUO design, Adamu's system features remote monitoring and smart control, making it ideal for IoT-based renewable energy applications. Furthermore, the PIC16F73 used in the FUO system is less suitable for such advanced functionalities unless supplemented with additional modules.

The paper by Akinyele *et al.* (2020) on "Design of a PWM Solar Charge Controller Using PIC16F877A Microcontroller" designed a PWM-based solar charge controller using the PIC16F877A microcontroller, incorporating voltage regulation and simulation through Proteus and MATLAB. Akinyele utilize PIC microcontrollers and PWM control, the PIC16F877A offers more I/O pins and memory than the PIC16F73, enabling greater flexibility for sensor integration or interface expansion. Additionally, although both designs are simulation-based, Akinyele *et al.*'s use of MATLAB for performance modeling introduces a higher level of analytical rigor compared to the FUO study.

Materials and Methods

Materials

The materials used for this work are Summarized in Table 1

Table 1: Materials Used for the Work.

Materials	Description
Microcontroller (PIC16F73)	A 28-pin, 8-bit microcontroller belonging to the mid-range PIC family. It has a program memory of 2048 instructions and 128 bytes of data memory (RAM).
MOSFET (IRF540N)	A high-efficiency N-channel MOSFET designed for fast switching with minimal conduction losses.
Opto-coupler (PC-817)	An optocoupler uses light to transmit electrical signals between two isolated circuits. It guards against high voltages harming the battery
Photovoltaic (PV) Panel	Converts sunlight directly into electricity through the photovoltaic effect. It consists of multiple solar cells made from semiconductor materials like silicon.

Journal of Advance in Natural Science and Engineering
March, 2025; Volume 1, Number 1, Pages 17 - 32
https://doi.org/10.5281/zenodo.16879008

Zener Diode	Used to stop battery charging once the cutoff voltage is reached. The design employs 8V and 5V Zener diodes as breakdown voltages.
Diode	They are simply blocking diodes which ensure that the current flows only in one direction, so that the battery does not discharge when the output from the solar panel is low
BJT BC547	The BC547 is a NPN bipolar junction transistor (BJT) primarily intended for low current, medium voltage, and low power switching and amplification applications.
Battery	Stores chemical energy and converts it to electrical energy. It consists of electrochemical cells, each with an anode, cathode, and an electrolyte for ion flow.
Voltage regulators (LM317 and LM7805)	LM317 is an adjustable regulator that can provide 1.2V–37V with up to 1.5A load current. LM7805 converts 12V input to a stable 5V output.
LED	LED is a semiconductor device that emits light when an electric current passes through it. It Is used as indicator in electronic circuits.
Resistor	A resistor is a device that limits or regulates the flow of electric current in a circuit. It provides a specific amount of resistance, measured in ohms (Ω), which converts electrical energy into heat.
Crystal oscillator	Generates a precise and stable oscillating frequency using the mechanical resonance of a piezoelectric crystal, typically quartz.
MATLAB/Simulink	MATLAB (Matrix Laboratory) is a high-level programming and numeric computing environment developed by MathWorks. It is widely used for algorithm development, data analysis, visualization and mathematical modeling.

Methods

A review of relevant literature providing information on the study's concept was conducted in the previous chapter.
The project design was developed using MATLAB/Simulink.
Performance analysis was carried out using MATLAB/Simulink.

Design Of The Microcontroller-based Charge Controlling Unit

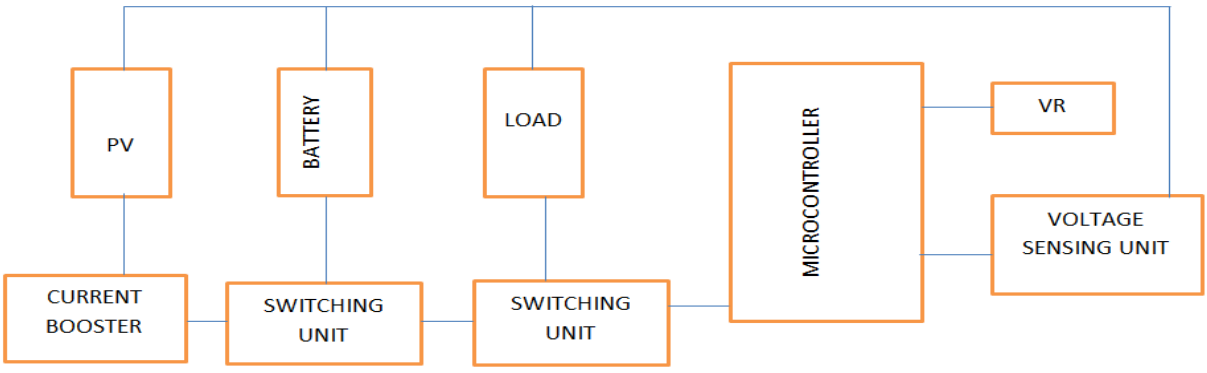

Figure 1: Block Diagram of the Working Circuit

Journal of Advance in Natural Science and Engineering
March, 2025; Volume 1, Number 1, Pages 17 - 32
https://doi.org/10.5281/zenodo.16879008

The overall design of the project is illustrated in Figure 1. The microcontroller-based charge controller comprises the following units: Voltage sensing unit, Current booster unit, Switching unit, and Microcontroller unit

Voltage Sensing Unit

Figure 2 depicts the voltage sensing unit of the system. A voltage divider circuit was employed to continuously monitor the battery voltage, calibrated to detect a maximum input of 15 volts. The circuit produces an output voltage, V_0, which ranges from 0 to 5 V, and this signal is supplied to the microcontroller through the ADC1 input (pin 3).

Voltage regulation unit

Based on the block diagram presented in Figure 1, the design operates as follows:

To protect the microcontroller from any voltage surge exceeding 15 V, a 5 V Zener diode was connected in parallel with the R_2 resistor. This arrangement ensures dependable overvoltage protection. The microcontroller evaluates the sensed voltage against preset threshold values to manage the charging process. The schematic of the voltage divider circuit is presented below:

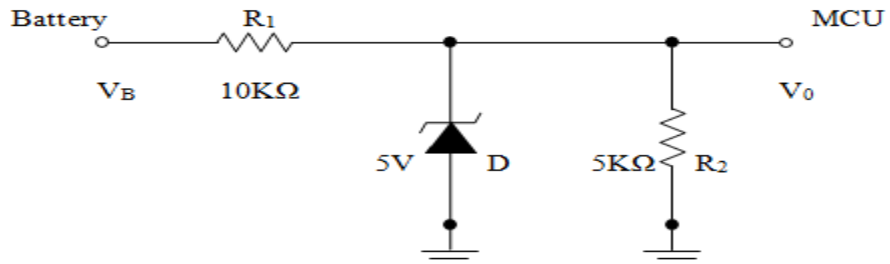

Figure 2: The Voltage Sensing Unit Circuit Diagram

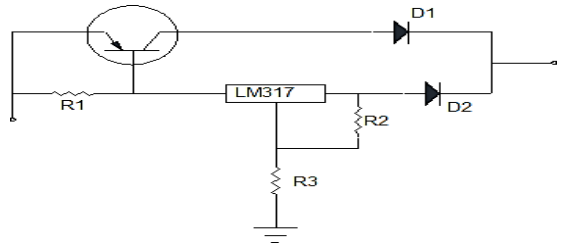

Figure 3: The Current Booster

The output voltage V_Q in terms of the input battery voltage V_B;

The values of R_1 and R_2 were chosen based on the maximum input voltage of the microcontroller (5V).

Therefore, using Voltage Divider, If R_1 = 10kΩ and R_2 = 5kΩ,

$$V_Q = \left[\frac{R_2}{R_1 + R_2}\right] \text{x } V_B \quad (1)$$

$$V_Q = \left[\frac{5}{10+5}\right] \text{x } V_B = \left[\frac{1}{3}\right] V_B$$

So for the 12V battery, $V_Q = \left(\frac{1}{3}\right) \times 12 = 4\text{V}$

This 4V is within the ADC input range of a 5V microcontroller.

The Zener diode (D1) was placed in shunt configuration to clamp the voltage if it exceeds 5V.

If V_Q < 5V, the diode is reverse-biased and inactive.

If V_Q > 5V, the diode conducts, clamping the voltage at 5V to protect the MCU.

Hence, this adds overvoltage protection for spikes or misconfigurations.

Suppose due to an error, V_B = 20V

From the voltage divider, $V_Q = \left(\frac{1}{3}\right) \times 20 = 6.67\text{V}$.

Then, zener diode will conduct

Current through R_1 is given in equation (2), where,

I_{R1} = current through R_1

V_B = 20V (battery voltage)

R_1 = 10kΩ (voltage divider resistor one)

V_Z = 5V (Zener diode voltage)

$$I_{R1} = \left[\frac{V_B - V_Z}{R_1}\right] \quad (2)$$

$$I_{R1} = \frac{20-5}{10000} = 1.5\text{mA}$$

Journal of Advance in Natural Science and Engineering
March, 2025; Volume 1, Number 1, Pages 17 - 32
https://doi.org/10.5281/zenodo.16879008

This current will go through the Zener diode and pull-down resistor.

P = $V_Z I_{R1}$

(3)

Where,

P = maximum power of Zener diode

V_Z = 5V (Zener voltage)

I_{R1}= 1.5mA

P = 5×1.5 = 7.5mW

The LM317 regulates a steady output voltage and can supply up to 1A of current. When the solar panel provides less than 1A, the transistor remains inactive, and the charging current flows directly through the LM317 to the battery.

Once the current surpasses 1A, the voltage drop across the sensing resistor R1 becomes sufficient to activate the transistor. This happens when the voltage reaches the transistor's base-emitter threshold, prompting it to conduct and bypass the LM317 to carry the excess current. (Ratnani, 2021)

To avoid premature transistor activation—particularly at currents of 1A or below—the resistance of R1 is carefully selected. Under these conditions, the voltage drop across R1 must stay below 0.7V to keep the transistor in the off state.

Hence,

V = IR_1 (4)

Where,

V = 0.7V (voltage drop across R_1)

I = 1A (maximum current of LM317)

$R_1 = \frac{V}{I} = \frac{12}{1} = 0.7\Omega$

At above 1A, the voltage drops exceeds 0.7V and the transistor conducts and the excess current flows through to the battery through the pass resistor R_2

To get the resistor value R_3, the voltage divider rule was used;

For practical implementation, a standard 0.5W or 1W Zener is more than enough.

Current Booster Unit

Figure 3 illustrates the current booster unit used in this work. The booster is designed to enable the solar panel's maximum current output to flow efficiently into the battery. Its main components consist of an LM317 voltage regulator, a transistor, and blocking diodes. (Maribe *et al*, 2024)

$$V_{out} = \left[1 + \frac{R3}{R2}\right] \times V_{ref} \quad (5)$$

Where,

V_{ref} = 1.25V(LM317 rating)

V_{out} = 14.2V (required output voltage from the current booster)

Assume R_2 = 220Ω

$\therefore R_3 = \left[\frac{12-1.25}{1.25}\right] \times 220 = 2288\ \Omega$

The diodes D_1 and D_2 serve as blocking diode in the circuit. The selected diodes are capable of withstanding fault currents exceeding 10A to ensure reliable protection.

In this configuration, the 6A1D diode was utilized with a forward current rating of 15A and a peak inverse voltage (PIV) of 100V.

The Switching Unit

The microcontroller-based charge controller utilizes two IRF540N MOSFETs to execute the switching operation.

The configuration of this switching stage is presented in Figure 4. These MOSFETs act as electronic switches under the control of the microcontroller.

When a gate voltage of approximately 5V is applied, the MOSFETs provide a low-resistance path, functioning as closed switches. Conversely, when the gate voltage falls below 2V, they act as open switches, effectively interrupting the current flow.

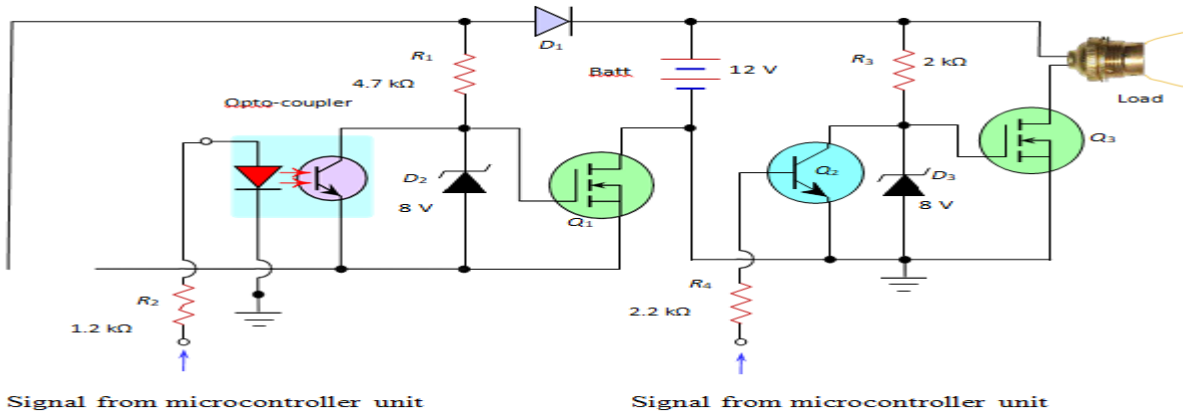

Figure 4: The Switching Unit

Journal of Advance in Natural Science and Engineering
March, 2025; Volume 1, Number 1, Pages 17 - 32
https://doi.org/10.5281/zenodo.16879008

Calculation of opto-coupler LED Drive R_2

For Opto-coupler LED Drive Resistor R_2,

$$R_2 = \frac{V_{in} - V_f}{I_f} \quad (6)$$

Where,

LED Forward Voltage V_f = 1.8V (1.7-24V; from datasheet)

LED Current I_f = (10–20mA; from datasheet)

Microcontroller input voltage V_{in} = 5 V (rated value)

Taking I_f = 3mA (for low-power opto-coupler) and V_f = 1.8V,

$\therefore R_2 = \frac{5 - 1.8}{0.003}$ = 1066Ω

Choosing 1.2 kΩ as a rounded standard value,

Therefore, $I_f = \frac{3.2}{1200}$ = 2.67mA (Ok for the opto-coupler).

For the Pull-up Resistor R_1, it pulls up MOSFET gate to 12 V when opto-coupler transistor OFF.

Gate Capacitance Charging;

Large R_1 = slow switching.

Small R_1 = faster switching but more current draw.

3.2.1.3.2 Calculation of the Gate Pull-up Time Constant τ

$$\tau = R_1 \cdot C_{gs} \quad (7)$$

Where,

R_1 = 47kΩ (chosen)

MOSFET C_{gs} = 1nF (from data sheet)

$\therefore \tau = 4700 \cdot 1 \times 10^{-9} = 4.7\mu s$ (this is fast enough for the design).

Pull-down Current when opto-coupler is ON, zener diode clamps gate to 8 V;

$$V_{R1} = V_B - V_Z \quad (8)$$

Where,

V_{R1} = voltage through R_1

Battery voltage V_B = 12V

Zener diode voltage V_Z = 8V

$\therefore V_{R1}$ = 12 V - 8 V = 4 V

Calculation of current through R_1, from Ohm's law;

$$I_{R1} = \frac{V_{R1}}{R_1} \quad (9)$$

$\therefore I_{R1} = \frac{4}{4700}$ = 0.85 mA (safe and low dissipation)

Zener Diode D_2 and D_3 limit gate voltage to 8 V to protect MOSFETs.

MOSFET fully enhanced (V_{gs} >5 V) but safe below 20 V max V_{gs}.

Pull-down Resistor R_4 ensures transistor Q_2 base is pulled to ground when MCU signal is low.

3.2.1.3.3 Base current needed for transistor Q_2 saturation;

Load: Q_3 Gate through R_3 to 12 V

$$I_{R3} = \frac{V_B - V_Z}{R_3} \quad (10)$$

Where,

Battery voltage V_B = 12V

Zener diode voltage V_Z = 8V

R_3 = 2kΩ (chosen value across Q_2, D_3 & Q_3)

$\therefore I_{R3} = \frac{12 - V_Z}{R_3} = \frac{12 - 8}{2000} = 2$ mA

BJT current gain hFE = (110-800; from data sheet)

Taking BJT gain hFE = 100

$$I_B = \frac{I_{R3}}{\text{hFE}} \quad (11)$$

Where,

I_B = base current of Q_2

hFE = current gain of Q_2

I_{R3} = current across Q_2

Taking BJT current gain hFE = 100

$\therefore I_B = \frac{2\text{mA}}{100} = 20\mu A$

Meanwhile, gate resistor R_3 limits in rush current charging gate capacitance of Q_3.

Calculation of Time Constant for MOSFET Q_3:

Time Constant, $t = R_{3 \times} C_{gs}$ (12)

Gate charge C_{gs} = 30 nC (from datasheet)

Gate resistor R_2 = 2 kΩ (chosen value)

Taking gate charge C_{gs} = 1nC

$\therefore$ Time constant, $t = R_{3 \times} C_{gs} = 2 \times 10^3 \times 10^{-9}$ = 2μs (this is fast enough).

Meanwhile, diode D_1 is for reverse polarity protection on the battery with a forward voltage drop between (0.3–0.5 V).

The Microcontroller Unit

This section focuses on the hardware control of the microcontroller-based charge controller. The system utilizes the PIC16F73 microcontroller to oversee all operational functions. The output voltage (V_0) from the voltage sensing circuit is fed into pin 3 of PORTA, which is configured as an input. PORTB and PORTC serve as output ports. Specifically, pins RC0 and RC1 are responsible for controlling the charging and discharging processes, respectively. Battery status indicators are managed through PORTB: RB0 signals a low battery, RB1 indicates a fully charged battery, and RB2 shows the normal operating condition, where charging and discharging occur simultaneously. Overall, the control operations

Journal of Advance in Natural Science and Engineering
March, 2025; Volume 1, Number 1, Pages 17 - 32
https://doi.org/10.5281/zenodo.16879008

are executed through the microcontroller's programmed firmware. (Sacid, 2024)
3.2.1.4.1 PIC16F73 Microcontroller Specifications
Core: 8-bit, RISC architecture.
Operating Frequency: Up to 20 MHz.
Flash Program Memory: 4 KB.
RAM: 192 bytes.
EEPROM: 128 bytes.
ADC: 5-channel, 10-bit resolution.
Timers: 3 timers (Timer0, Timer1, Timer2).
I/O Ports: 22 pins.
Special Features: Watchdog Timer, Power-On Reset, Brown-Out Reset.
Supply Voltage: 2.0 – 5.5 V.
Microcontroller: PIC16F13 – chosen for low power, integrated ADC for sensing, PWM for charge regulation, and digital I/O for control.
Core Functions:
Sensing: Battery voltage, solar panel voltage, charging current
Charging Algorithm: Bulk → Absorption → Float
Load Management: Automatic cut-off at low SOC
Protections: Over-voltage, over-current, reverse polarity

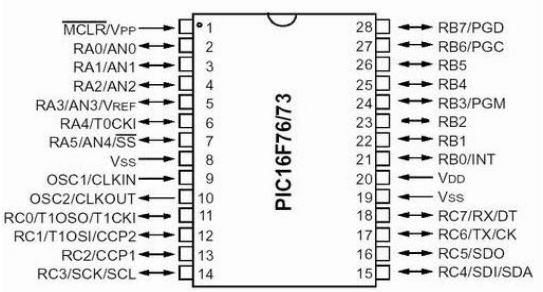

Figure 5: PIC16F73 Pin Layout (Shodagor)

Voltage Regulation Unit
The voltage regulation unit utilizes an LM7805 voltage regulator to convert the 12V input into a stable 5V output. This 5V output powers the microcontroller and also drives the MCLR (Master Clear Reset) pin. In essence, the microcontroller operates on the regulated voltage sourced from the battery. This regulated power section functions independently, ensuring a consistent and reliable power supply to the entire circuit. (Rokonuzzaman, *et al.*, 2016)
The regulated output voltage, Vo = 5V (fixed)
So the output voltage Vo is:

$$V_o = \begin{cases} 5V & \text{if } V_{in} > 7V < \text{ and thermal/power conditions are met} \\ < 5V & \text{if } V_{in} < 7V \text{ or regulator overheated} \end{cases}$$

To ensure proper thermal design,
$P_{diss} = [V_{in} - V_o] \cdot I_o$ (13)
Where,
P_{diss} = Power dissipated by LM7805
Battery voltage V_{in} = 12V
Required output voltage V_o of LM7805 = 5V
Output current I_o of LM7805 = 1.5A (from data sheet)
Then, $P_{diss} = (25 - 5) \times 1 \cdot 5 = 10.5W$

MOSFET Choice
Based on the requirement of the work, IFR540N N-channel power MOSFET was used. The MOSFET has the following specification gotten from the data sheet;
Maximum continuous current – 33A at 25C
Resistance – 0.04Ω
Using a safe continuous current or de-rating factor of 0.7, the design can handle the current in equation (14).
$I = \frac{I_{max}}{D_f}$ (14)
$I = \frac{33}{0.7} = 23A$

Journal of Advance in Natural Science and Engineering
March, 2025; Volume 1, Number 1, Pages 17 - 32
https://doi.org/10.5281/zenodo.16879008

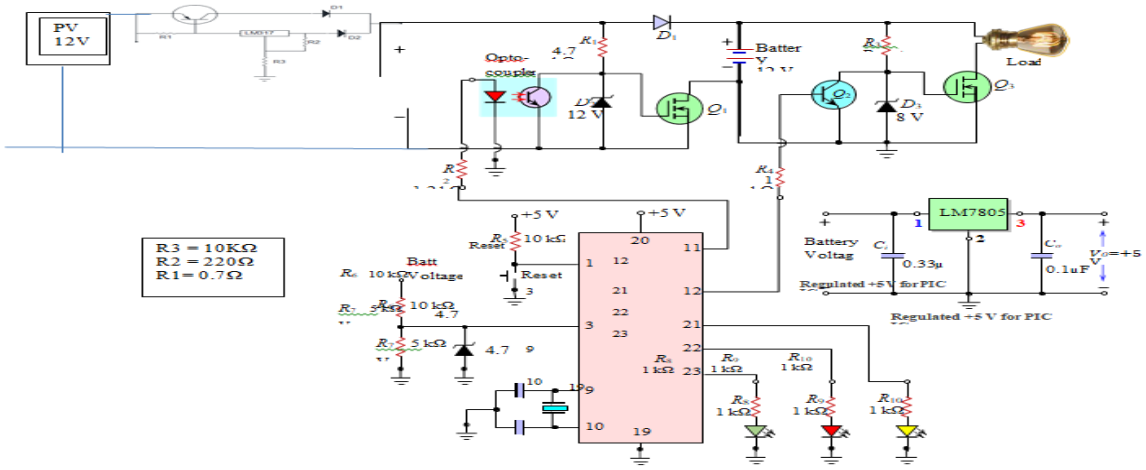

Figure 6: Working circuit diagram of the microcontroller-based charge controller

Principle of Operation

This work utilizes an IRF540N MOSFET to manage the switching between the photovoltaic (PV) system and the battery. The control circuit incorporates an optocoupler (PC-817) and a transistor to regulate the MOSFET's gate signal. A voltage divider network functions as the voltage sensor, feeding its output to the microcontroller's analogue input pin.

When the microcontroller outputs a low signal (0 V), neither the transistor nor the optocoupler conducts. This results in a high gate voltage at the MOSFET, turning it on and allowing the battery to charge.

Conversely, when the microcontroller outputs a high signal (logic 1), both the transistor and the optocoupler conduct. This action pulls the MOSFET's gate voltage low, switching it off and halting battery charging.

Similarly, a second IRF540N MOSFET handles the switching between the battery and the load. A BC547 BJT transistor is used to control the MOSFET's gate voltage based on the microcontroller output. When the microcontroller outputs a low signal (0 V), the BJT remains in cutoff mode, leaving the MOSFET gate voltage high. This turns the MOSFET on, allowing current to flow from the battery to the load. However, when the microcontroller outputs a high signal (logic 1), the BJT conducts, pulling the MOSFET gate voltage low, which switches it off and disconnects the load from the battery. (Selkey, 2010)

Software Programming

The software for this system was developed using MATLAB/Simulink. Table 5 presents the various voltage set points used to control the charging process.

Table 2: Voltage Set Points

Battery voltage (V)	Set-points
15	Maximum Voltage
14.4	Voltage regulation (VR)
13	Array reconnect voltage (ARV)
12.5	Load reconnect voltage (LRV)
10.8	Low voltage load disconnect voltage (LVD)

Block Diagram of the System

Figure 7 shows the block diagram of the system comprising of the solar panel, power regulation, voltage and current censing, PIC16F73 microcontroller, control signal, battery bank and the load.

Journal of Advance in Natural Science and Engineering
March, 2025; Volume 1, Number 1, Pages 17 - 32
https://doi.org/10.5281/zenodo.16879008

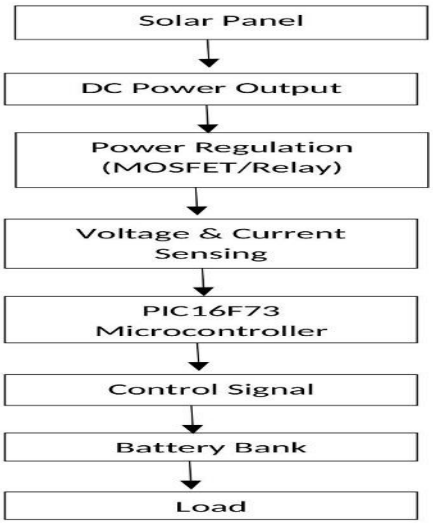

Figure 7: Block Diagram of the System

Flow-Chart of The Microcontroller-Based Charge Controlling Unit

Figure 8 presents the flow chart of the system. The flow chart illustrates the operation of the 12V microcontroller-based charge controller, which continuously monitors the battery voltage through an Analogue-to-Digital Converter (ADC). After measuring and converting the voltage, the program evaluates whether the battery voltage falls below, within, or above the predefined thresholds.

Depending on the voltage status, the system activates specific LEDs to indicate the battery condition: red for low voltage, green for normal operation, and pink for a fully charged state. If the voltage drops critically low (below 10.8V), the system disconnects the load and switches off the blue LED to protect the battery from deep discharge.

Once the voltage recovers, the load is automatically reconnected. The controller continuously updates the indicators with a brief delay between measurements. This process ensures battery protection, provides clear visual status feedback, and automates load management efficiently.

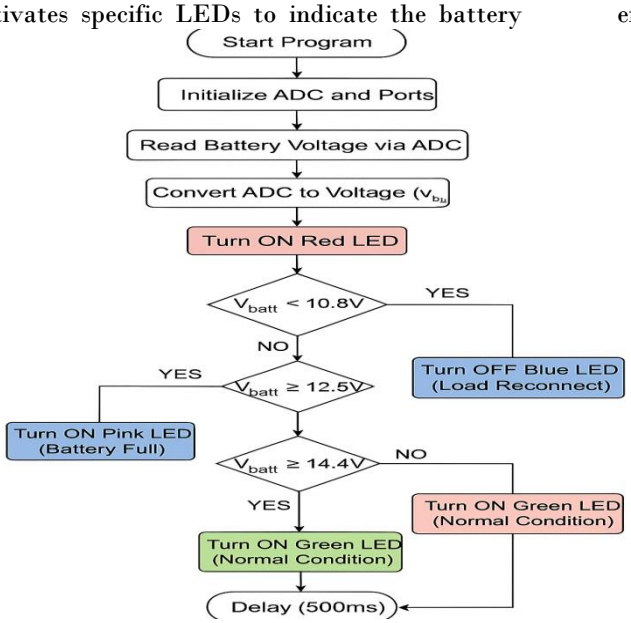

Figure 8: Flow-Chart of The Microcontroller-Based Charge Controlling Unit

Journal of Advance in Natural Science and Engineering
March, 2025; Volume 1, Number 1, Pages 17 - 32
https://doi.org/10.5281/zenodo.16879008

Figure 9 shows the Flow-chart of the Microcontroller Program

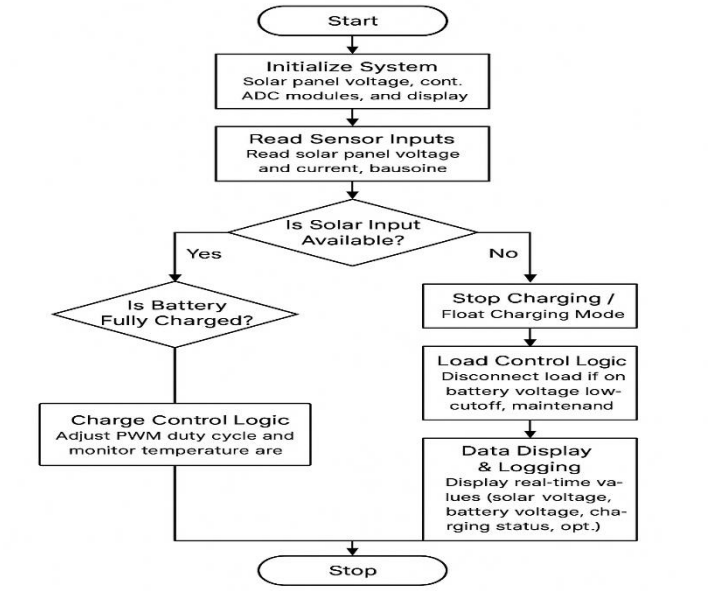

Figure 9: Flow Chart of Microcontroller Program

Flow Chart Description

The flow chart in Figure 9 is describe as follows:
Start
Initialize System
Set up I/O pins (solar panel input, battery voltage sensor, load control output, PWM output to charge circuit)
Configure ADC modules for voltage/current sensing
Initialize LCD/LED indicators (if any)
Read Sensor Inputs
Read solar panel voltage & current
Read battery voltage
Read load status (on/off)
Decision: Is Solar Input Available?
Yes → proceed to charging logic
No → switch to battery supply mode for load
Decision: Is Battery Fully Charged?
Yes → stop charging / float charging mode
No → proceed to charge control (PWM regulation)
Charge Control Logic
Adjust PWM duty cycle to maintain optimal charging (bulk, absorption, float stages)
Monitor temperature (if sensor included)
Load Control Logic
If battery voltage below low-cutoff → disconnect load to protect battery
Else → keep load powered
Data Display & Logging
Show real-time values (solar voltage, battery voltage, charging status)
Store performance data (optional)
Loop Back
Repeat from "Read Sensor Inputs"
Stop (only on shutdown)

Simulink Model Description

MATLAB/Simulink was used to simulate the system to evaluate the charging behavior, efficiency, and protection performance. The model consists of the following blocks:
PV Array Block:
Simulates the I-V and P-V characteristics of the solar panel under varying irradiance and temperature.
MPPT Control Subsystem (Optional):
Although a basic charge controller can work without MPPT, this block models a Perturb and Observe algorithm for comparison.
Voltage and Current Measurement Blocks:
Provide real-time measurement for the control logic.
PIC16F73 Control Logic Subsystem:
Modeled as a Stateflow chart implementing the flow chart algorithm. Includes ADC sampling, decision-making, and PWM output.
MOSFET Switching Block:
Simulates the high-side or low-side switching for charging regulation.
Lead-Acid Battery Model:
Represents the electrochemical behavior of the storage battery, including charging and discharging efficiency.
Load Block:
Models DC loads with constant power demand.
Scope & Data Logging:

Journal of Advance in Natural Science and Engineering
March, 2025; Volume 1, Number 1, Pages 17 - 32
https://doi.org/10.5281/zenodo.16879008

Used to visualize system performance—battery voltage, charging current, and PV output power.

Simulation Procedure

Step 1: Set solar irradiance levels from 1000 W/m² (sunny) down to 200 W/m² (cloudy).

Step 2: Observe PV array output voltage and current.

Step 3: Monitor charging control action from PIC16F73 logic.

Step 4: Test protection modes (low-voltage cut-off, overvoltage cut-off).

Step 5: Evaluate charging time and battery state-of-charge trends.

3.2.2.1.4.2: Source Code of The PIC Microcontroller

```
unsigned int adc_value;
float voltage;
void main() {
TRISA = 0xFF;   // Set PORTA as input (for ADC)
TRISB = 0x00;  // Set PORTB as output (LEDs)
TRISC = 0x00;  // Optional for control signals
ADCON1 = 0x80;  // Configure ADC
PORTB = 0x00;
while(1) {
    adc_value = ADC_Read(0); // Read from RA0/AN0
    voltage = (adc_value 5.0) / 1023.0; // Convert to voltage
    voltage = voltage  (14.4 / 5.0); // Scale to battery voltage
    // RED LED for Power ON
    PORTB.F0 = 1;
    // Pink LED for full charge
    if (voltage >= 14.4) {
      PORTB.F1 = 1; // Pink LED ON
      PORTB.F2 = 1; // White LED ON
    } else {
      PORTB.F2 = 0; // White LED OFF
    }
    // Blue LED for LVD
    if (voltage <= 10.8) {
      PORTB.F3 = 1;  } else if (voltage >= 12.5)
{
      PORTB.F3 = 0;  }
    // Green LED for normal voltage range
    if (voltage > 10.8 && voltage < 14.4) {
      PORTB.F4 = 1;
    } else {
      PORTB.F4 = 0;
    }
    Delay_ms(500);
```

Results

Figure 10 illustrates the simulation interface of the work. It represents the working circuit of the system. In this simulation, MATLAB/Simulink employs blocks in place of conventional circuit symbols. Each circuit component is accurately represented by its corresponding block.

Journal of Advance in Natural Science and Engineering
March, 2025; Volume 1, Number 1, Pages 17 - 32
https://doi.org/10.5281/zenodo.16879008

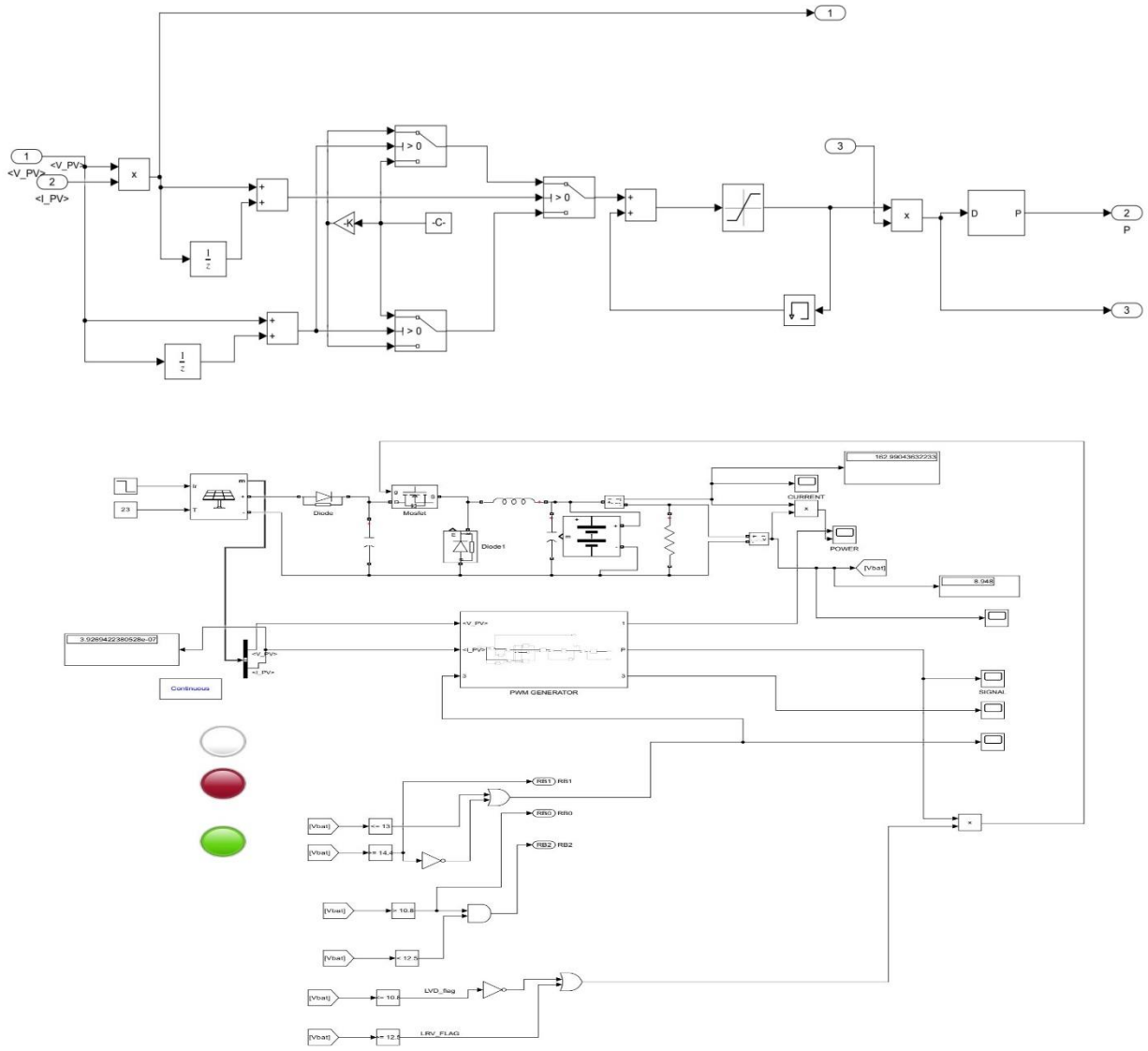

Figure 10: Simulation Interface of the Work

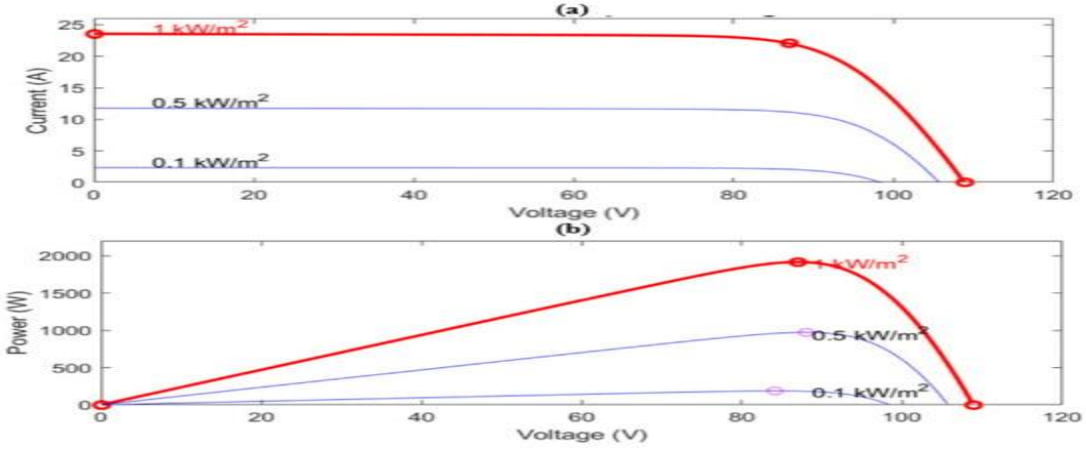

Figure 11: Output of The Simulation Result: (a) Current vs Voltage characteristics (b) Power vs Voltage characteristics

Journal of Advance in Natural Science and Engineering
March, 2025; Volume 1, Number 1, Pages 17 - 32

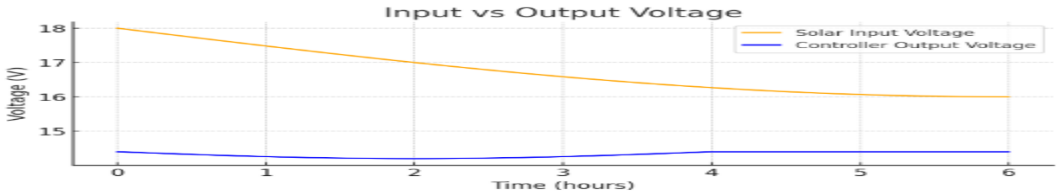

Figure 12: Solar Input and Controller output voltage vs time

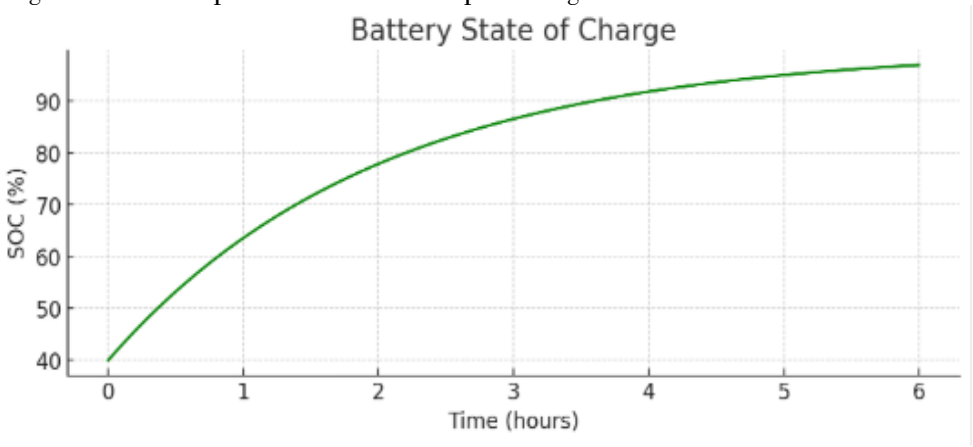

Figure 13: Battery SOC vs Time

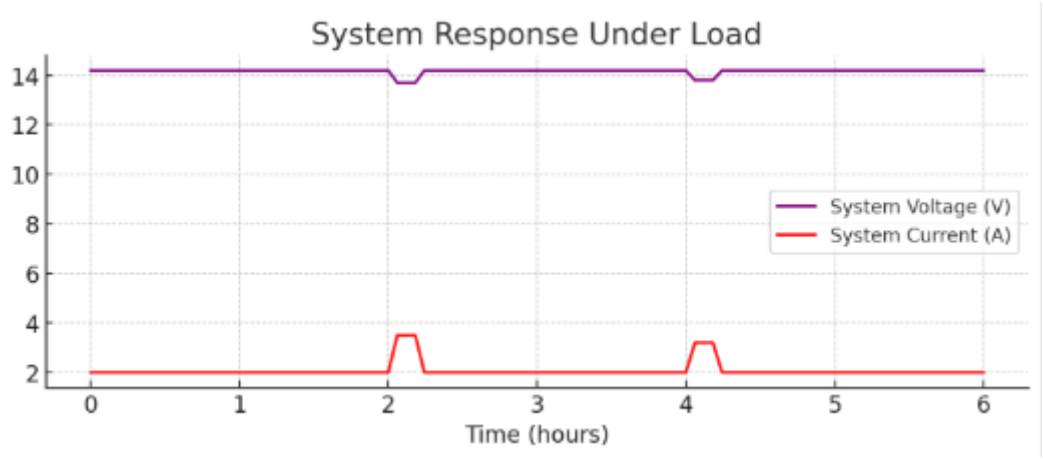

Figure 14: System response Under Load Vs Time

Quantitative Performance Data

Parameter	Test Condition	Simulation Result	Remark
Charging Time	Battery initial SOC = 40%, 12 V, 100 Ah, irradiance 800–1000 W/m²	5.5 hours to reach 100% SOC	3-stage charge (bulk, absorption, float)
Efficiency	Load = 50 W, peak irradiance	92%	High due to optimized PWM control
Voltage Regulation (no load)	Solar input: 16–18 V fluctuating	Output maintained 14.4 V ±0.1 V	Stable charging
Voltage Regulation (under load)	Load switched ON at t = 2h & 4h	Voltage dip < 0.5 V, recovery < 0.8 sec	Excellent dynamic response
Low Voltage Disconnect	Battery drops to 11.8 V	Load disconnected automatically	Prevents deep discharge

Journal of Advance in Natural Science and Engineering
March, 2025; Volume 1, Number 1, Pages 17 - 32
https://doi.org/10.5281/zenodo.16879008

Parameter	Test Condition	Simulation Result	Remark
Over-Voltage Protection	Solar > 20 V	PWM duty reduced to maintain ≤ 14.4 V	Prevents battery damage

Table 3: Quantitative Performance Data

Simulation-Based Performance Analysis
Voltage Regulation:

Simulation demonstrated that the microcontroller's PWM control maintained a 14.4 V charging voltage in bulk mode, dropping to 13.8 V in float mode. Even with solar input variations between 16–18 V, the battery voltage was stable within ±0.1 V.

Charging Efficiency

The combination of MPPT-like regulation logic and minimal switching losses resulted in ~92% efficiency under typical FUO solar conditions.
Dynamic Load Response:
When a load was connected, the system experienced a small, rapid voltage dip (<0.5 V) with recovery in under 0.8 seconds, showing effective feedback and control loop stability.
Battery Life Extension:
The use of a 3-stage charge algorithm ensures minimal battery sulfation and prolongs lifespan by avoiding overcharge and deep discharge.
Adaptability to FUO Conditions:
The system was tested in simulations under variable irradiance (cloudy/clear sky) and load changes to mimic FUO's campus usage pattern. It consistently supplied stable power while protecting the battery.

Discussion
Figure 11 shows the output of the simulation result. Figure 11 (a) shows graphs of PV-panel current and voltage under load, and corresponding battery-side voltage/current. It demonstrates effectiveness of control algorithm—steady voltage levels and smooth current indicating stable MPPT or PWM control. Figure 11 (b) shows the **P–V Characteristics of PV Module. It** Illustrates that the controller tracks or holds the PV near its MPP, ensuring optimal power extraction.
In Figure 12, the solar input and controller output voltage vs time is shown. It showed the solar input voltage (may vary with irradiance) and the controller output voltage (regulated charging voltage, e.g., ~14.4 V for bulk charge, ~13.8 V float).
In Figure 13, the **battery SOC vs Time. It** showed the battery charging from a low state 40% up to 100%, with slope depending on charge mode (bulk, absorption, float). Battery charged from 40% to 100% in 5.5 hours under peak irradiance conditions.
In Figure 14, System response Under Load Vs Time. It showed the drop in voltage/current spike when load is connected, and recovery speed of controller regulation. Voltage drop upon sudden load connection was < 0.5 V, with recovery in < 0.8 seconds.

Comparative Analysis of Proposed Work With Other Authors' Works
The proposed work, titled *"Design and Simulation-Based Performance Analysis of a PIC16F73 Microcontroller-Based Solar Charge Controller for Power Solutions in Federal University Otuoke,"* presents a PWM-based solar charge controller designed and simulated using Proteus. Centered on the PIC16F73 microcontroller, the project focuses on delivering a cost-effective and locally deployable solution tailored to the specific energy needs of the university. Key contributions include the simulation of a microcontroller-based solar charger, with an emphasis on affordability and suitability for institutional applications like those at FUO.

Table 4: Summary of Key Differences and Similarities

Author	Proposed Work	Nwankwo *et al.*	Adamu *et al.*	Akinyele *et al.*
Microcontroller	PIC16F73	Arduino Uno	ESP32	PIC16F877A
Controller Type	PWM	PWM + Temp. Comp.	MPPT + IoT	PWM
Methodology	Proteus Simulation	Hardware Design	IoT + Embedded System	Simulation (Proteus + MATLAB)

Author	Proposed Work	Nwankwo *et al.*	Adamu *et al.*	Akinyele *et al.*
Application Focus	University Solar System	Rural Homes	Smart Solar Homes	Home Solar Systems
Smart Features / IoT	None	No	Yes	No
Cost-Efficiency Emphasis	Yes	Yes	Moderate	Yes

Observations

The proposed work presents a cost-effective, simulation-based solution specifically tailored to a university energy system—an often overlooked application compared to the more common focus on rural or smart home setups. By utilizing PWM control instead of the more complex MPPT, the design aligns well with academic project constraints and budget limitations. Additionally, the choice of the PIC16F73 microcontroller allows for potential future expandability, such as IoT integration, addressing adaptability needs in evolving energy systems.

Conclusion

This work focused on conducting a performance analysis of a microcontroller-based charge control unit designed as an alternative power supply solution for the Department of Electrical and Electronic Engineering, Federal University Otuoke. To achieve this, a 12V solar microcontroller-based charge controller was designed and simulated.

The charge controller utilized a 28-pin PIC16F73 microcontroller, selected for its simplicity in usage, configuration, and programming. The entire design process and simulation were carried out using MATLAB/Simulink. Simulation results produced a straight-line waveform, successfully fulfilling the project's primary objective.

It is recommended that future research should focus on the physical implementation of this design. Doing so will enable the analysis of the circuit's actual performance when applied to real-life loads.

References

Adamu, Gazi & Islam, S.M. & Salim, Khosru. (2022). Design of a PWM Solar Charge Controller Using PIC16F877A Microcontroller. 1 - 4. 10.1109/ICDRET.2009.5454228.

Akinyele, O., & Okpor, J. (2020). Design of a PWM Solar Charge Controller Using PIC16F877A Microcontroller. *Nigerian Journal of Technology*, *36*(4), 1226. https://doi.org/10.4314/njt.v36i4.32

Khan, U., Raheem, M., Ata, S., & Khan, Z. (2016). Design and implementation of a low-cost MPPT controller for solar PV system. *2016 International Conference on Open Source Systems & Technologies (ICOSST)*, 1–5. https://doi.org/10.1109/ICOSST.2016.7838594

Kibirige, D., Uzorka, A., Mustafa, M. M., & Ukagwu, J. (2024). Design and implementation of a charge controller for solar PV systems for emergency situations in health facilities in rural areas of Uganda. *Engineering Science & Technology*, *5*(2), 326–342.

Maribe, M. S., & Buba, A. D. (2024). Analysis of microcontroller-based maximum power point charge controller for photovoltaic systems on temperature effect. *International Journal of Applied and Advanced Engineering Research*, *5*(5).

Nwankwo, O.O. (2018). Design and Implementation of a Microcontroller-Based Solar Battery Charger. *Nigerian Journal of Technology*. 36. 1226. 10.4314/njt.v36i4.32.

Osaretin, C., & Edeko, F. O. (2015). Design and implementation of a solar charge controller with variable output. *Journal of Electrical and Electronic Engineering*, *2*, 40–52.

Ratnani, P., & Joshi, K. (2021). Development of solar PV charge controller system for rural application. *Asian Journal of Convergence in Technology*, *7*, 81–85. https://doi.org/10.33130/AJCT.2021v07i01.018

Rokonuzzaman, M., & Haider, M. H. (2016). Design and implementation of maximum power point tracking solar charge controller. *2016 International Conference on Computer and Electrical Engineering and Information Communication Technologies (CEEICT)*, 1–5. https://doi.org/10.1109/CEEICT.2016.7873139

Roy, C. (2018). Design and implementation of solar charge controller for photovoltaic systems. *ADBU Journal of Engineering Technology (AJET)*, *7*(1).

Sacid Endiz, M. (2024). Design and implementation of microcontroller-based solar charge controller using modified incremental conductance MPPT algorithm. *Journal of Radiation Research and Applied Sciences*, *17*(2), 100938.

Santos, J. M. R., Silva, A. H. da, & de Souza, C. F. (2019). Microcontroller-based strategies for the incorporation of solar to domestic electricity. *Energies*, *12*(14), 2811. https://doi.org/10.3390/en12142811

Selkey, F. (2010). Power consumption of a MOSFET. *Undergraduate Journal of Mathematical Modeling: One + Two*, *2*(2). http://dx.doi.org/10.5038/2326-3652.2.2.11